



High-density direct laser deposition (DLD) of CM247LC alloy: microstructure, porosity and cracks

Prveen Bidare¹ · Aldi Mehmeti¹ · Amaia Jiménez² · Sheng Li¹ · Chris Garman³ · Stefan Dimov¹ · Khamis Essa¹

Received: 13 December 2021 / Accepted: 23 April 2022 / Published online: 7 May 2022
© The Author(s) 2022

Abstract

Nickel-based alloys are known as non-weldable materials due to their complex characteristics. Consequently, additive manufacturing of these alloys is particularly challenging. In this paper, the influence of process parameters on the porosity, crack formation and microstructure of additively manufactured CM247LC nickel-based alloy is analysed. The feasibility of the direct laser deposition (DLD) process to manufacture crack-free and low-porosity CM247LC samples is studied. CM247LC samples were built on Inconel 718 that has similar chemical composition, to form hybrid superalloy parts. It was shown that crack-free and high-density CM247LC samples can be obtained through DLD without significant substrate preheating for certain parameter combinations: laser power in the range of 800–1000 W and powder feed rates between 6 and 8 g/min. High-cost and complex preheating was avoided that was commonly reported as necessary to achieve similar densities. For hybrid parts, a large beam diameter and slow scan speeds were employed to achieve optimal conditions as it was evident from the achieved bonding between the Inconel 718 substrate and the deposited layers. It was observed that good bonding between the two materials can be obtained with laser power values between 800 and 1000 W, scanning speed higher than 300 mm/min and powder flow rates of 6–8 g/min.

Keywords Additive manufacturing · Nickel-based superalloys · Porosity · Microstructure

1 Introduction

Nickel-based alloys provide unique properties such as good mechanical and chemical resistance to degradation in harsh environments and when subjected to thermal exposures, due to the precipitation of γ' and γ'' strengthening phases [1, 2]. These properties make them suitable for applications in the aerospace and energy industries [3, 4]. Among these alloys, the present work focuses on the CM247LC alloy that is a chemically modified version of the more common MAR M247 and was particularly developed for blade and vane applications [5]. The modifications on its chemical composi-

tion provide this alloy with improved castability, ductility, fatigue strength and carbide stability [6, 7]. However, like other nickel-based alloys, the additive manufacturing (AM) of CM247LC components is particularly challenging. It is known as a non-weldable material due to its high Nb, Al and Ti content [8] that entails various cracking mechanisms including solidification, liquation, strain age, ductility-dip cracking and hot cracking [1, 7]. These issues are due to the high thermal gradients between the substrate and deposited material, mechanical constraints, the complex grain boundaries and the precipitate strengthening of these alloys [9, 10]. As a consequence, AM of crack-free and fully dense CM247LC components is still a matter of research.

Studies in the literature have been focused on the optimisation of AM parameters to achieve the best results. It has been shown that AM enables the generation of parts with tensile strength and elongation similar or even better than those achieved by conventional processing, although special attention must be paid to the combination of parameters employed. Laser power, laser spot diameter, scanning speed and scanning strategy have a significant influence on the properties of the generated components [4, 11]. Energy density must be enough to ensure proper melting of

✉ Prveen Bidare
p.bidare@bham.ac.uk

✉ Khamis Essa
K.E.A.Essa@bham.ac.uk

¹ School of Mechanical Engineering, University of Birmingham, Birmingham, UK

² TECNUN Escuela de Ingeniería, Universidad de Navarra, Manuel de Lardizábal 15, 20018 San Sebastián, Spain

³ MBDA UK Limited, Six Hills Way, Stevenage, Hertfordshire SG1 2DA, UK

materials, but excessive input thermal load may lead to the formation of unstable melt pools [12]. Pleass and Jothi [13] added the characteristics of powder as another factor that influences the properties of manufactured components. In this regard, MacDonald et al. [9] analysed the influence of particle size and characteristics on the microstructure and mechanical properties of laser power bed fusion (L-PBF) CM247LC after HIP treatment. They observed that fine powders promote the formation of certain boundaries that are detrimental to the mechanical properties of AM components. They also noted that a wide range of particle size distribution (0–150 μm) provided the best balance of properties at high temperatures. Weng et al. [14] analysed the influence of powder feeding rate and scanning velocity on microstructure and tensile properties of wire-based DED of 316L stainless steel. They observed that, for an optimised combination of laser power, powder feed rate and scanning speed, the process enabled the formation of dual austenite/ferrite microstructure samples with high tensile strength and good performance in terms of plastic deformation.

Although a great effort has been made to optimise AM process parameters, these technologies still present some issues that need to be addressed. AM nickel-based components exhibit microstructural defects as high crystallographic texture, columnar grain structure and intergranular defects that affect their mechanical behaviour. They also present high residual stresses, deformations due to thermal distortions, poor surface quality, ageing issues and anisotropic mechanical properties [15–17]. Additionally, the appearance of cracks is another issue to consider [11]. Residual stresses generated and the rapid cooling rates that are common when employing these technologies intensify the cracking tendency of these alloys [2]. Initial defects such as gas pores, shrinkage porosity, inhomogeneous microstructure and lack of fusion might be responsible for the initiation of cracks under loading conditions [18]. Due to the mentioned issues, AM samples are usually subjected to post-process heat treatments or HIPing to reduce cracking occurrences and improve porosity which, in turn, improves their mechanical behaviour [19, 20]. In their work, Bhaduri et al. [21] evaluated the feasibility of L-PBF technology to generate bi-material components and it was observed that tensile properties of parts had improved after annealing and ageing heat treatment. In addition to heat treatments, the feasibility of machining operations to improve the accuracy and properties of AM components has also been analysed recently by researchers [15, 21–25]. As an example, in the work conducted by Careri et al. [26], heat treatments and machining operations were combined as post-processing techniques to direct laser deposited (DLD) nickel-based components. They noted that the machinability of DLD and then heat-treated components is comparable to that of conventionally

manufactured components. Regarding the benefits of this post-processing technique, authors observed that by increasing cutting parameters, the surface qualities can be improved.

Other methods have also been proposed in literature to avoid the formation of cracks in AM of superalloys. Seidel et al. [1] proposed a different approach to avoid hot cracking during DLD of nickel-based alloys that included heating the substrate through induction. This led to a decrease of the temperature gradient between the substrate and the melt pool and, therefore, the thermally induced stresses could be controlled. The authors obtained crack-free samples with the proposed methodology. The use of a pulsed laser was the solution proposed by Imbrogno et al. [27] to improve the metallurgical characteristics of Inconel 718 alloy. The authors noted that the formation of Nb-rich phases (known as Lave) during the welding process that occur in AM increases the tendency to crack formation due to the brittle nature of this phase. They observed that by using a pulsed laser, less Nb is segregated, which in turn can reduce cracks development.

It can be stated that AM of nickel-based alloys and particularly CM247LC alloy is still an active research field. Concretely, the optimisation of process parameters to obtain best results in terms of porosity, crack formation and mechanical properties of printed components needs further investigation. It has been shown that, in most cases, substrate preheating or post-processing treatments (heat treatments or machining operations) are needed to obtain high-quality, fully dense and crack-free CM247 AM samples, which is time consuming. Additionally, these processes are sometimes hard to accomplish due to the complex geometries and high-added values of the AM components.

Given this context, the present work is aimed to find DLD process parameter ranges that enable the formation of fully dense and crack-free samples without the need of preheating and/or post-processing operations through auxiliary equipment, as previously proposed by different research groups. In this regard, a series of experimental tests are conducted with varying process parameters to analyse their influence on porosity, crack formation and microstructure and in this way to understand better the process. Based on those results, a range of process parameters is provided that ensures a good performance of the DLD process and enables the generation of CM247 components with good properties. The work is also aimed at studying the feasibility of using the DLD technology for repair of nickel-based components. Considering this, a second set of experiments is conducted with Inconel 718 as substrate material and the bonding between deposited CM247 material and Inconel 718 substrate is analysed in detail.

Table 1 Composition (wt. %) of the CM247LC powder used in this research

C	Al	Ti	Cr	Mo	Hf	Ta	Co	W	B	N	O	O (supplier)	Ni
0.09	5.57	0.80	8.29	0.61	1.31	3.10	9.59	9.57	140 ppm	< 20 ppm	< 100 ppm	75 ppm	Bal

2 Materials and methods

DLD tests were conducted on Mazak Integrex i-400AM hybrid machine [28]. This machine integrates the DLD technology into a 5-axis machining setup. The laser employed in this hybrid manufacturing centre is 1 KW single-mode laser with 1.064 μm wavelength. The AMBIT high-rate deposition head from Hybrid Manufacturing Technologies was used. On the substrate, a beam spot size of 2 mm was achieved with a 10-mm standoff distance. A large laser beam diameter was selected because it has been shown to improve laser-based AM processes because of the beneficial effects on the conduction welding regime that is more stable and enables the generation of almost fully dense parts [29]. During the experimental tests, shield gas pressure, shield gas flow rate, nozzle gas flow rate and carrier gas flow rate were set to 1.5 bar, 10 l/min, 10 l/min and 6 l/min, respectively. A first operation was run before deposition with a defocused beam was performed before the deposition to evaporate grease, coolant, oil and other possible residues from the substrate surface. No major change in substrate temperature was noticed due to this process. The chemical composition of the CM247LC powder employed during the experiments is provided in Table 1.

In Fig. 1, the morphology and particle size distribution of the CM247LC powder used in the experiments are shown. It can be seen in Fig. 1a that the powder has a mainly spherical morphology, dendritic structure on surfaces and satellite particles that are typical in gas-atomised powders. Additionally, according to the size distribution (Fig. 1b), the powder can be considered unimodal as no noteworthy peak can be identified in the distribution with $d_{50} = 63 \mu\text{m}$.

Preliminary tests were conducted to obtain a range of process parameters that ensure a good performance of

the deposition process. Multi-track deposition tests were later accomplished on Inconel 718 substrates using the processing window that was identified with the conducted preliminary trials.

After deposition, all samples were sectioned, ground and polished for a follow-up analysis. The samples were sectioned in the cross and longitudinal directions (XZ and YZ) as shown in Fig. 2.

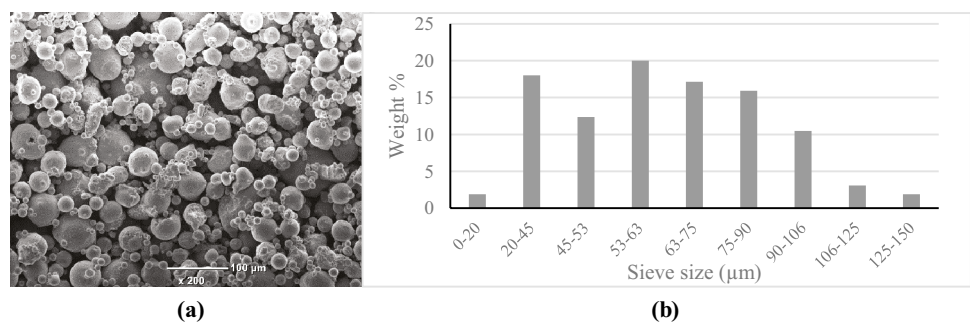
In order to analyse the influence of different process parameters on the microstructure, porosity and bonding of samples, images from both sections were taken using Hitachi TM3030 SEM equipment. The images were later analysed using ImageJ software. Regarding the analysis of experimental data, the influence of different process parameters on the microstructure, porosity and bonding of samples was studied. To analyse the influence of laser heat input, as suggested by Read et al. [30], the so-called energy density ψ was calculated as follows for different process parameter combinations:

$$\Psi = \frac{P}{f_r \cdot h \cdot t} \tag{1}$$

where P being the laser power, f_r is the scanning speed, h is the hatching space and t is the deposited layer thickness. The influence of other parameters such as the energy input per unit length (E_L [J/mm]), the applied powder mass per unit length (G [mg/mm]) and the specific energy (E_m [J/mg]) on porosity of samples was also analysed. These parameters were suggested by Hentschel et al. [31] to analyse the influence of laser-related and process-related parameters on the obtained results in AM and they can be calculated as follows:

$$E_L = \frac{P}{f_r} \tag{2}$$

Fig. 1 CM247LC powder characteristics: **a** SEM image of powder morphology and **b** particle size distribution



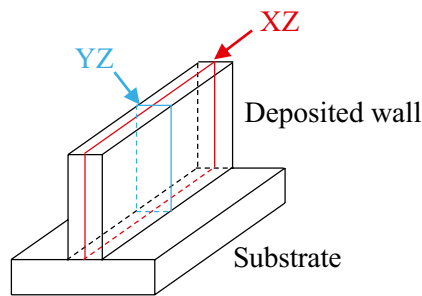


Fig. 2 Sections conducted to analyse the microstructure and porosity of DLD samples

$$G = \frac{\dot{m}}{f_r} \quad (3)$$

$$E_m = \frac{E_L}{G} = \frac{P}{\dot{m}} \quad (4)$$

where \dot{m} being the powder flow rate.

According to the experimental tests, single-track depositions were first conducted with varying process parameters to find a window for optimal DLD conditions that lead to smooth tracks with no internal cracks or porosity. A wide range of laser power, scan speed and powder flow rate values were employed in order to analyse the influence of all variables on the obtained deposition characteristics.

Multi-layer deposition tests were conducted next with the parameter combinations that demonstrated the optimum results in the preliminary tests. These parameters are provided in Table 2.

The 30 mm long and ~20 mm in height ribs that are shown in Fig. 3 were generated during multi-layer tests on SS304 substrate. Once the samples were created, microstructure, porosity and crack formation in the deposited material were analysed. Subsequently, the best parameters that gave crack-free high-density builds were further used to deposit CM247LC powder on IN718 substrates. Special attention was paid to the boundaries between the substrate and the first deposited layers in order to evaluate the bonding of CM247LC onto Inconel 718.

Fig. 3 Multiple-track samples of CM247 deposited on 304SS substrate (a) wall 1-9, (b) wall 10-17 and (c) wall 18-25

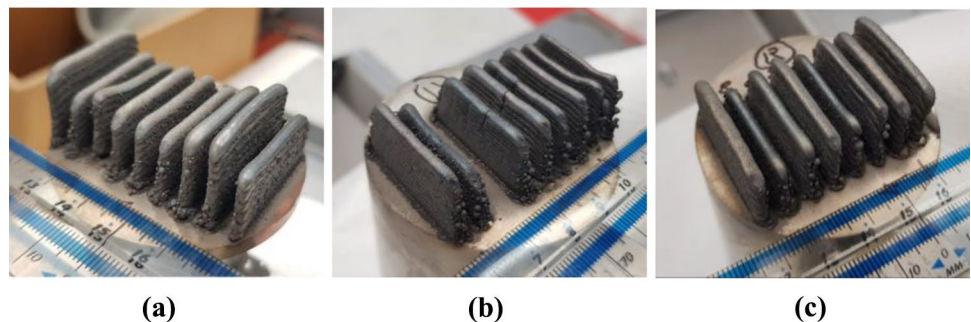


Table 2 Process parameter values employed in the multi-layer tests

Parameter	Lower level	Mid-level	Higher-level
Laser power (W)	600	800	1000
Scan speed (mm/min)	200	300	400
Powder flow rate (g/min)	6	8	10

3 Results and discussion

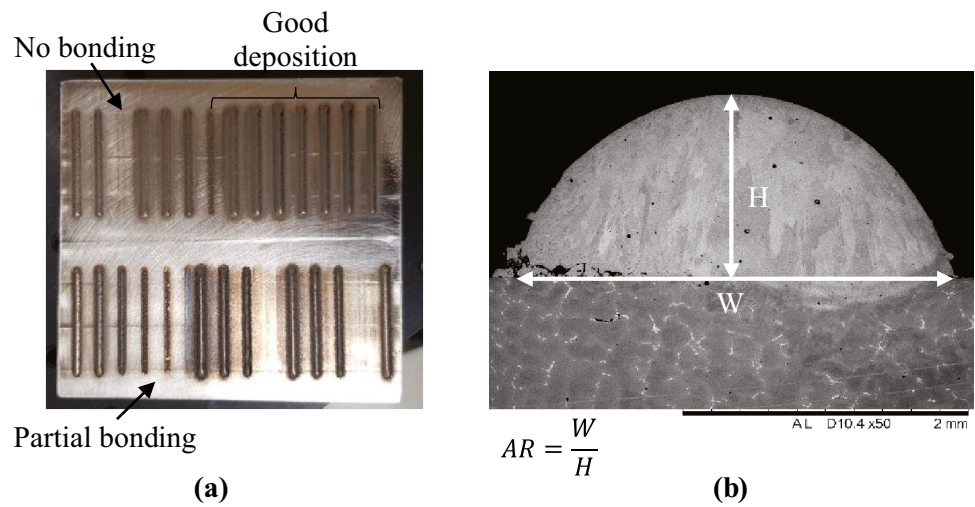
Results obtained in the conducted experiments are presented next. First, the influence of process parameters on achieved aspect ratios of single-track samples is analysed. Then, the analysis of porosity, crack formation and microstructure of these samples is conducted. Finally, the analysis of boundaries between the Inconel 718 substrate and deposited CM247LC is presented.

3.1 Analysis of preliminary trials

Figure 4a shows the single-track samples deposited in 304SS substrate during the preliminary trials with different process parameters. Depending on the parameters used, different results were obtained regarding the bonding (no bonding, partial bonding or good bonding) to the substrate. In addition, the morphology of the deposited tracks was evaluated by calculating the achieved aspect ratios (AR), i.e. the ratio between the width (W) and the height (H) in the YZ cross section of a single-track sample as shown in Fig. 4b. It is commonly accepted that depositions with AR between 3 and 6 exhibit adequate bonding. However, in this study, as suggested by Shamsaei et al. [32], only parameter combinations that led to aspect ratios between 2 and 4 were considered optimal.

To give an overview of the effects of varying process parameters on AR achieved, Fig. 5 provides the SEM images of the YZ cross section of analysed single-track CM247LC samples deposited on 304SS substrate. It was possible to identify a range of parameters that can lead to depositions with optimal AR. Concretely, high laser power value (above 800 W), scanning speeds between 200 and

Fig. 4 Single-track samples: **a** whole length of the samples and **b** SEM image of the YZ cross section of one of the samples with achieved AR



400 mm/min and powder feed rates between 4 and 10gr/min showed best results. Additionally, those processing windows led to crack-free and dense depositions.

It is observed in Fig. 5 that for 200 m/min scanning speed, if low laser power ($P=600$ W) and low laser feed rates ($FR=3$ g/min) are employed, AR of the deposited layer is 5. However, by using this same scanning speed ($S=200$ m/min), combined with a higher laser power ($P=800$ W) and a slightly higher powder feed rate ($FR=4$ g/min), an $AR=4$

is obtained that is considered within the optimal range. As known, laser power directly influences the temperatures achieved in the melt pool; therefore, it has a major influence on the melting processes and the obtained density. Additionally, scanning speed can also influence the temperature achieved on the melt pool, its geometry and the cooling rate and solidification process once the layer is deposited. Finally, it is observed that powder flow rate must also be taken into account to optimise process parameters. If a high

Fig. 5 AR values obtained in single-track DLD experiments on 304SS substrate with investigated process parameters

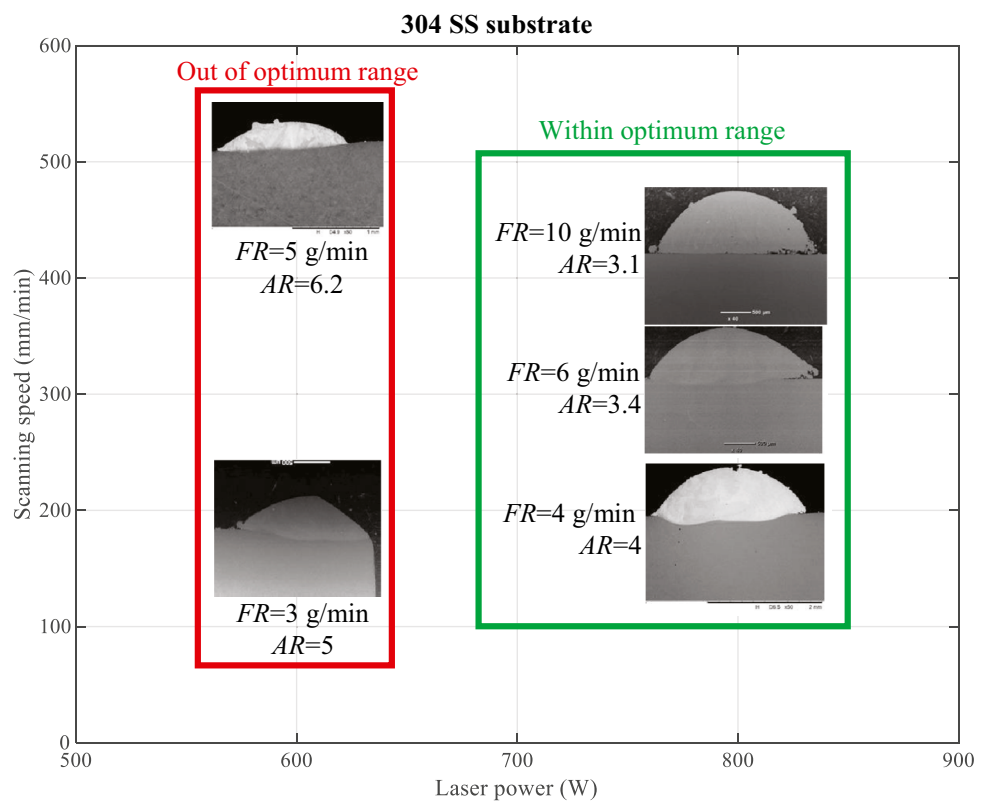
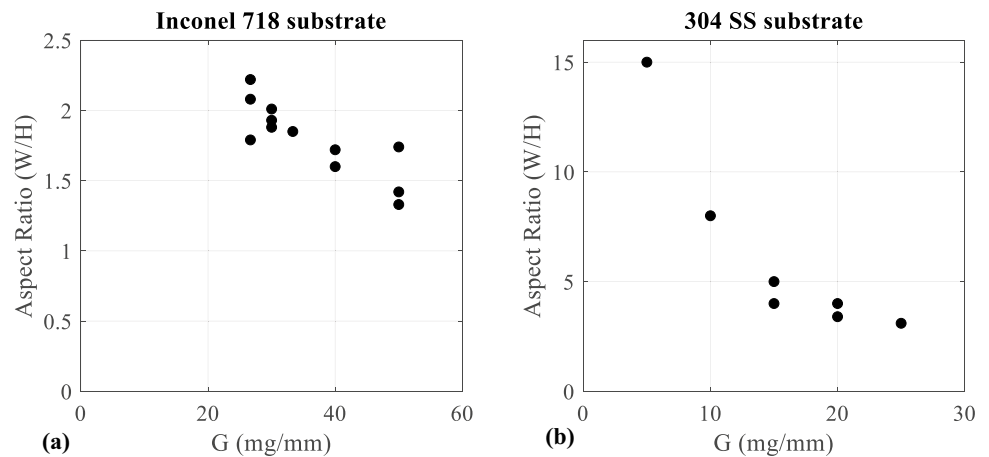


Fig. 6 Influence of the applied powder mass per unit length G on AR of single-track samples deposited on **a** Inconel 718 and **b** 304SS substrates



powder flow rate is selected, enough heat input to properly melt all the powder must be ensured. Therefore, based on the results shown in Fig. 5, the need for an analysis of the combined influence of process parameters on the resulting AR was stated.

The influence of process parameters on AR of single-track samples was analysed for all parameter combinations investigated in this research, considering both substrate materials. A similar set of single-track CM247LC samples were produced on Inconel 718 substrate. Figure 6 shows the evolution of AR with respect to the applied powder mass per unit length G (3) for the two substrate materials investigated in this research that gives a general view of their influence on achievable AR .

It can be stated that regardless of the substrate material, the aspect ratio of single-track samples decreases with the increase of the applied powder mass per unit length G .

3.2 Analysis of the deposited material

3.2.1 Influence of process parameters on microstructure

Figure 7 shows SEM images of CM247LC bulk obtained from the YZ cross section of different rib samples deposited on 304SS substrate.

The parameter values employed to generate the ribs shown in Fig. 7a, b led to the formation of cracks. Both samples were deposited with high energy input (800 W laser power) and the morphology of the cracks that appear is the typical solidification cracking that occurs in those cases [33]. These high values led to a fast cooling rate that is the reason for crack formation. At the same time by analysing Fig. 7c, d, it can be stated that a higher laser power leads to improved density of the produced samples. The porosity in the sample included in Fig. 7c is due to lack of fusion that occurs when power is not enough to melt powder properly. Higher laser power induces a better melting of the powder, therefore, enables the formation of more dense ribs. Another possible

reason for the appearance of this spherical porosity is a bad shielding that leads to the so-called gas trapped porosity. During the depositions, local shielding was employed, which in some cases might not be enough to ensure optimal deposition conditions.

Regarding the microstructure of the samples, it was observed that columnar and directional microstructure with elongated grains oriented along the build direction can be obtained (see Fig. 7d) when high laser power and low scanning speeds are used. This is a consequence of the slow solidification that is the result of the applied combination of parameters. In fact, comparing Fig. 7b, d, it is seen how scanning speed affects the solidification. It is seen that a decrease in scanning speed provides more time to a better solidification and enables the generation of a crack-free sample.

Also, by analysing the images in Fig. 7, it can be noted that a window of parameters can be identified (Fig. 7d) for 304SS substrate that lead to crack-free and high-density CM247LC samples with good microstructural properties. In this regard, high laser power (above 800 W) and intermediate scanning speeds (300 mm/min) that enable a good solidification have shown the best results.

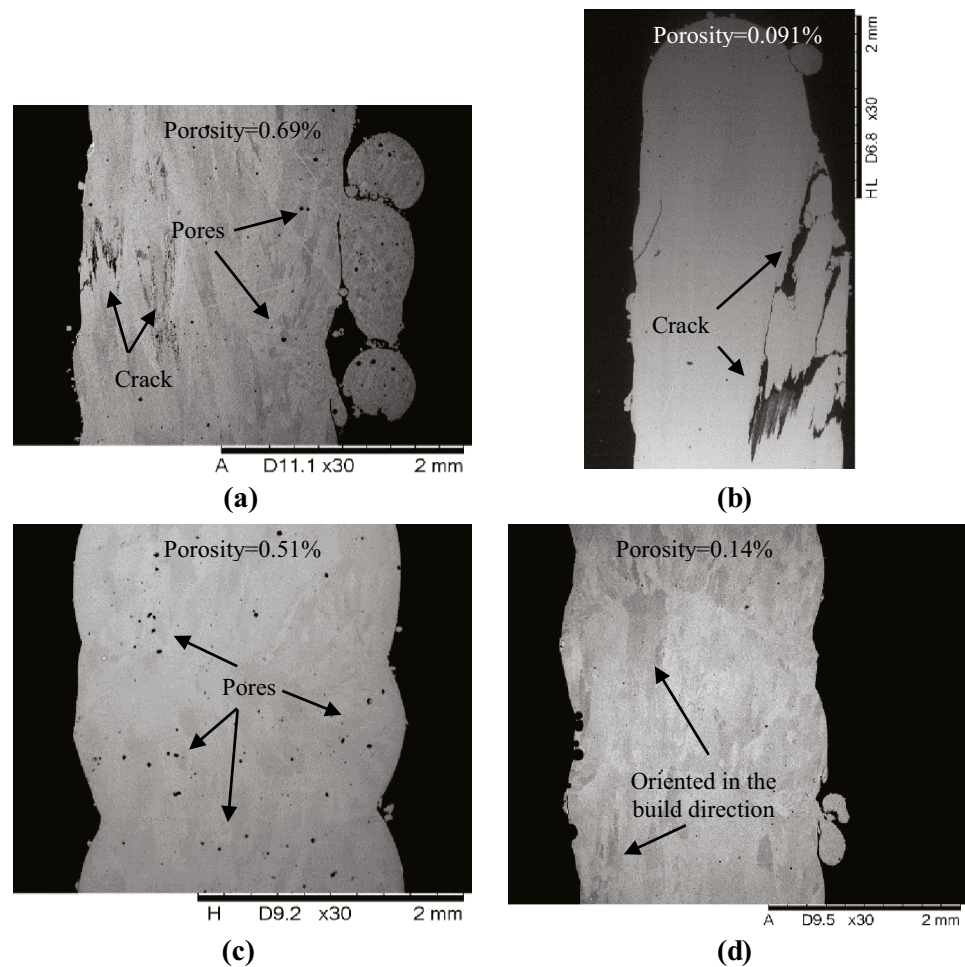
In Fig. 8, SEM images of the same samples previously shown in Fig. 7 are included, but in this case with their corresponding XZ cross sections of the ribs.

By comparing Figs. 7 and 8, it can be stated that similar results have been obtained in both directions. Therefore, only the images and values corresponding to the transversal cross-sectional (YZ) cuts are included and discussed further.

Figure 9 shows the SEM images of CM247LC ribs produced on Inconel 718 substrate.

Analysing the SEM images, it can be stated that the samples shown in Fig. 9a–c do not depict an optimal microstructure. In particular, the low laser power used for the samples in Fig. 9a, b is not sufficient to fuse the powder and thus pores are formed in the lattice. Additionally, if a higher scanning speed is employed (Fig. 9b, c), the

Fig. 7 SEM images of the YZ cross section of the ribs produced on 304SS using different process parameters: **a** 800 W, 400 mm/min, 10 gr/min; **b** 800 W, 400 mm/min, 8 gr/min; **c** 600 W, 200 mm/min, 6 gr/min; and **d** 800 W, 300 mm/min, 8 gr/min



deposited layer cannot solidify sufficiently before the following one is deposited. The heat load generated during the deposition of successive layers leads to side effects that are similar to heat treatments. As a result, a coarse microstructure is formed that entails low nucleation rates and a continuous grain growth in the structure. Furthermore, if the powder melting is not adequate, cracks can be generated during the process (see Fig. 9c). On the other hand, deposition parameters employed in Fig. 9d led to a defect-free microstructure, with only a marginal amount of pores. In this case, a columnar, directional and elongated grain microstructure along the build direction can be seen. The columnar grains are a consequence of the temperature gradients in the build direction, which is typical for AM components. Additionally, the large size of the grains is attributed to the slow solidification that, in turn, is a consequence of the lower scanning speed employed, i.e., 200 mm/min. Lastly, the grain orientation reflects the scanning strategy employed during the deposition, especially the zig-zag growth orientation as seen in the cross section (Fig. 9b), that is attributed to the continuous motion of the laser that is typical in the CW regime.

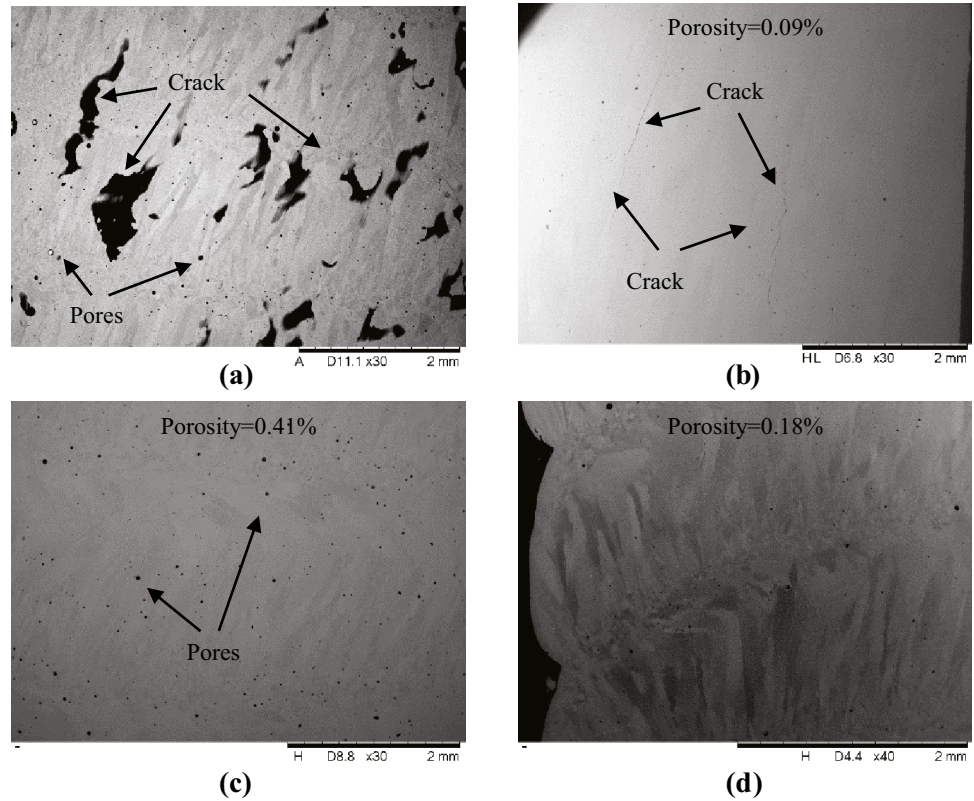
3.2.2 Influence of process parameters on porosity

Firstly, the influence of laser power (P), scanning speed (S) and powder flow rate (FR) on bulk porosity was analysed independently. Figure 10 shows the evolution of bulk porosity in CM247 deposited on Inconel 718 (dashed lines) and 304SS (continuous lines) substrates with varying parameters.

As expected, porosity decreases with the increase of laser power as it is shown in Fig. 10a. However, the opposite trend is observed with increasing powder flow rate in Fig. 10c. As laser power increases, the heat input increases and, therefore, an adequate melt pool is generated that reduces the formation of pores during the deposition. However, if the heat input is fixed, the increase of powder flow rate leads to higher porosity. This can be explained with no sufficient heat input to melt all delivered powder. Additionally, an excessive amount of powder can obstruct the laser beam resulting in poor melting. Finally, the influence of scanning speed on porosity is not clear for both substrate materials.

The effect of parameters' combinations on porosity was also investigated. Figure 11 shows the evolution of the porosity

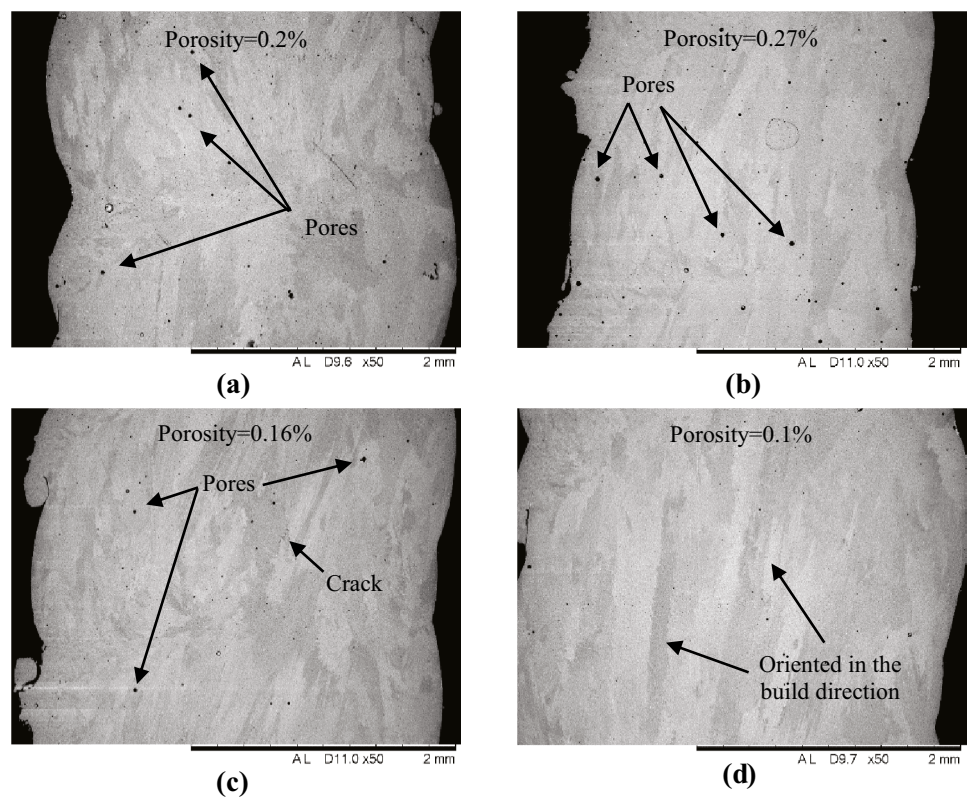
Fig. 8 SEM images of the XZ cross section of the ribs produced on 304SS using different process parameters: **a** 800 W, 400 mm/min, 10 gr/min; **b** 800 W, 400 mm/min, 8 gr/min; **c** 600 W, 200 mm/min, 6 gr/min; and **d** 800 W, 300 mm/min, 8 gr/min



of CM247LC walls ribs deposited on Inconel 718 substrate with respect to the energy density ψ that combines the effects of laser power and scanning speed. It can be seen in

the figure that porosity decreases with an increase in energy density. Again, this can be attributed to the increase of heat input that facilitates the melting of all delivered powder.

Fig. 9 SEM images of the YZ cross section of ribs produced on Inconel 718 using different process parameters: **a** 800 W, 200 mm/min, 6 gr/min; **b** 800 W, 300 mm/min, 8 gr/min; **c** 1000 W, 300 mm/min, 8 gr/min; and **d** 1000 W, 200 mm/min, 6 gr/min



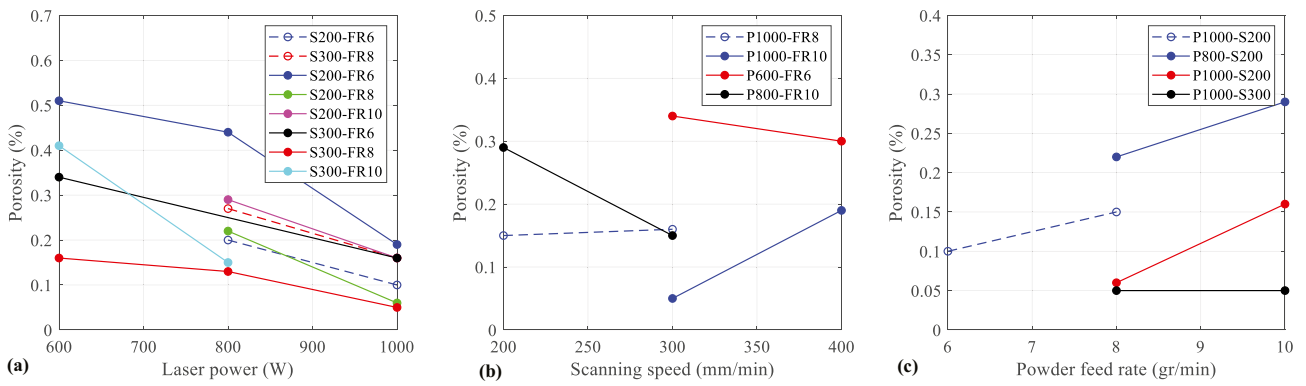


Fig. 10 The influence of process parameters on porosity of the deposited bulk, especially the effects of **a** laser power, **b** scanning speed and **c** powder flow rate

3.3 Analysis of the boundaries between the substrate and deposited layers

As it was already mentioned, a special attention was paid to the analysis of substrate/layer boundaries of samples deposited on Inconel 718 to investigate the potential application of DLD for the repair of nickel-based superalloys' components. The bonding between the substrate and first deposited layers was analysed by evaluating the so-called bonding ratio between the width of the adequately bonded material and the total width of the boundary between them. Figure 12 depicts the boundaries between Inconel 718 substrate and the first CM247LC layers for two sets of deposition parameters. It can be seen that the process parameters affect the resulting bonding, too. It was evident that low laser power (Fig. 12a) led to certain regions of

the deposition (marked with arrows) to not bond to the substrate adequately. At the same time, high laser power (Fig. 12b) resulted in a better welding of deposited layers to the substrate.

To analyse the influence of each process parameter independently on the bonding performance, the evolution of the bonding ratio was analysed with varying processing parameters as shown in Fig. 13. The effects of each parameter on the bonding ratio were analysed while keeping the other two constant. The information about the values of the fixed processing parameters in each experiment is included in the figure legend.

It can be seen in Fig. 13a that bonding improves with the increase of laser power, while it decreases with the increase of powder flow rate (Fig. 13c). The effect of laser power on the bonding performance is due to the increase of the heat input that enables a better melting of materials and, in turn, a better welding between the substrate and the deposited layers. Regarding the scanning speed, no clear interdependence between the bonding performance and scanning speed can be identified in the obtained results in Fig. 13b. Further research needs to be carried out to understand the effect of scanning speed on the bonding performance. It should be noted that the scanning speed affects the width of the layers, as its increase deduces their thickness. However, no relation with the bonding performance has been previously reported. As for the powder flow rate, it can be stated that the weldability of materials degenerates when higher volumes of powder are delivered. Therefore, to maintain the bonding performance with the increase of the flow rate, it would be necessary to increase heat input in order to melt all delivered powder properly. In addition, if powder flow rate is too high, it might obstruct the laser beam and lead to an inadequate melting and bad bonding between materials.

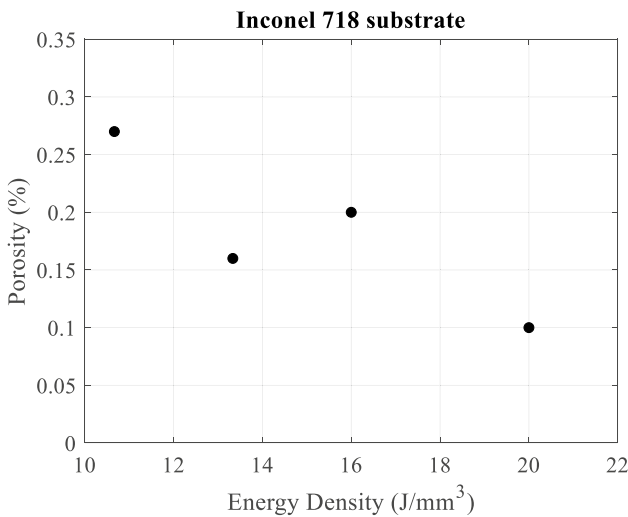


Fig. 11 The effect of energy density on porosity of deposited ribs

Fig. 12 SEM images of the boundaries between Inconel 718 substrate and first layers deposited with the following processing parameters: **a** 600 W, 200 mm/min, 10 gr/min, and **b** 1000 W, 200 mm/min, 10 gr/min

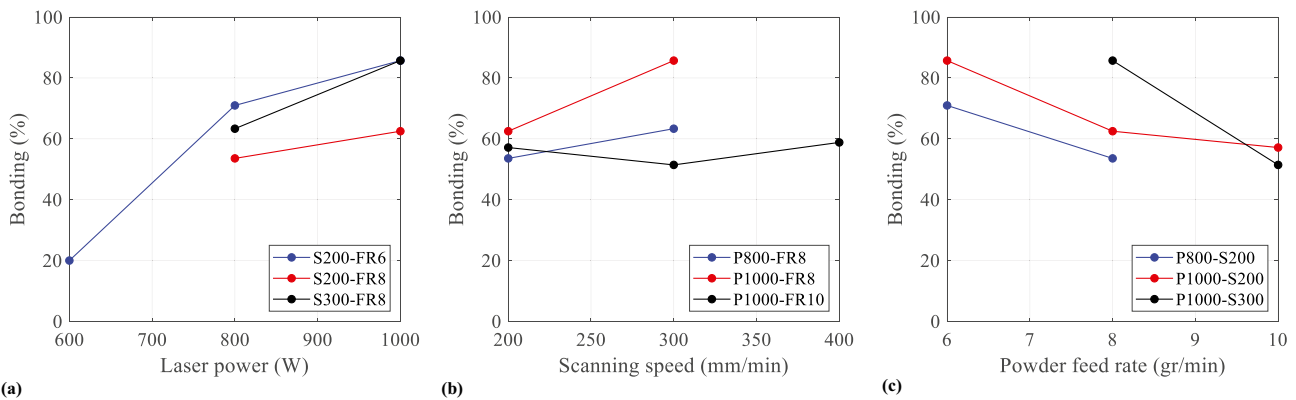
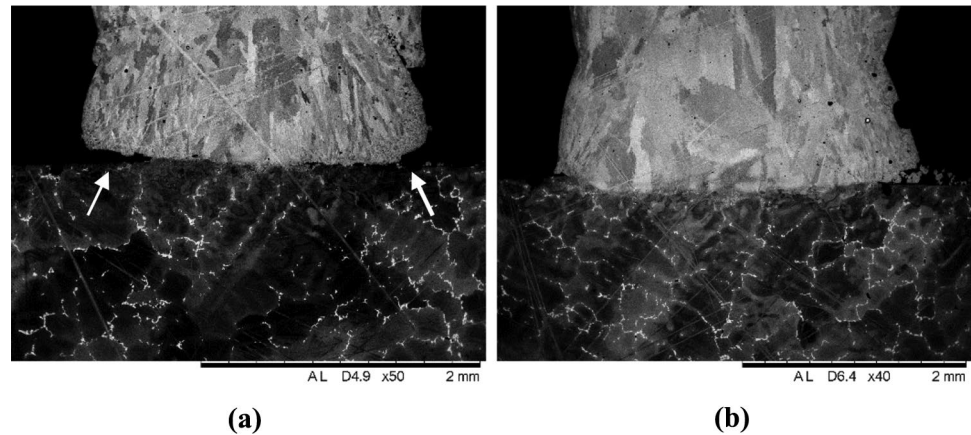


Fig. 13 The effects of processing parameters on the bonding performance, i.e. the influence of **a** laser power, **b** scanning speed and **c** powder flow rate

4 Conclusions

The paper reports an investigation of DLD process parameters' effects on microstructure, porosity and crack formation in CM247LC samples deposited on Inconel 718 and 304SS substrates. Additionally, the boundaries between the Inconel 718 substrate and the deposited layers were analysed to investigate the potential use of this technology for repair of nickel-based alloys' components. The main reason to use 304SS substrates for the initial trials was its relatively low cost, availability and better machinability. After the initial trial on the 304SS substrate, the optimal parameters were subsequently used on IN718 substrates to investigate the achievable bonding performance with the DLD process. The influence of laser power, scanning speed and powder flow rate on the porosity, crack formation and microstructure of samples produced on both substrate materials was analysed. Lastly, the feasibility of deploying the DLD process for repairing Inconel 718 components by using CM247LC powder was also investigated. Special attention was paid to

the interface between the Inconel 718 substrate and deposited CM247LC layers, to analyse the achievable bonding performance while varying the processing parameters. From the results obtained, the following conclusions can be drawn in this research:

- There is a certain range of deposition parameters that enable the build-up of pore-free and crack-free CM247LC samples by employing the DLD technology without any substrate preheating and/or part post-processing. One of the main reasons for this is the use of a large diameter laser beam and low scanning speeds.
- Regarding the effects of process parameters on the microstructure of the deposited ribs, it can be stated that high laser power and low scanning speed lead to a columnar and directional microstructure with elongated grains oriented in the build direction. This can be attributed to the good melting and successive solidification of the deposited material that, in turn, is due to the high heat input and sufficient cooling time, respectively.

- The influence of process parameters on the resulting porosity was also analysed. As expected, it was observed that porosity decreases with the increase of laser power. However, the powder flow rate has the opposite effect on porosity. The high powder flow rate led to higher porosity. It can be also stated that scanning speed did not have a clear effect on the porosity for the range of investigated processing parameters.
- As for the achieved bonding between the nickel-based alloys, it has been determined that good results can be obtained when a certain range of process parameters are used. Thus, it can be stated that the DLD of CM247LC can be considered a potential option for the repair of Inconel 718 components.
- The increase of laser power and powder flow rate led to a better bonding between deposited CM247LC lasers and the Inconel 718 substrate. However, scanning speed did not have a clear effect on the bonding performance within the range of deposition parameters investigated in this research.

In addition to the conclusions listed above, it has been noted that time gap between consecutive layers has also an important influence on the quality of depositions. Therefore, further research will be carried out in the future to analyse this and find the optimal time delay constant.

Acknowledgements The authors thank the financial support provided by the MBDA UK Limited for the IC061 project under the MCM ITP Innovation research program. This work has been performed by the University of Birmingham in partnership with MBDA, the Defence Science and Technology Laboratory (Dstl) and the Direction générale de l'armement (DGA), and funded under the Materials and Components for Missiles, Innovation and Technology Partnership (MCM ITP).

Funding This study was funded by the MBDA UK Limited, IC061 project, under the MCM ITP research program.

Declarations

Ethics approval This paper is our original unpublished work, and it has not been submitted to any other journal for reviews.

Consent to participate All authors were fully involved in the study and preparation of the manuscript; each of the authors has read and concurs with the content in the final manuscript.

Consent to publish All authors consent to publish the content in the final manuscript.

Competing interests The authors have no relevant financial or non-financial interests to disclose. The authors have no conflicts of interest to declare that are relevant to the content of this article. All authors certify that they have no affiliations with or involvement in any organization or entity with any financial interest or non-financial interest in the subject matter or materials discussed in this manuscript. The authors have no financial or proprietary interests in any material discussed in this article.

Open Access This article is licensed under a Creative Commons Attribution 4.0 International License, which permits use, sharing, adaptation, distribution and reproduction in any medium or format, as long as you give appropriate credit to the original author(s) and the source, provide a link to the Creative Commons licence, and indicate if changes were made. The images or other third party material in this article are included in the article's Creative Commons licence, unless indicated otherwise in a credit line to the material. If material is not included in the article's Creative Commons licence and your intended use is not permitted by statutory regulation or exceeds the permitted use, you will need to obtain permission directly from the copyright holder. To view a copy of this licence, visit <http://creativecommons.org/licenses/by/4.0/>.

References

1. Seidel A, Finaske T, Straubel A, Wendrock H, Maiwald T, Riede M, Lopez E, Brueckner F, Leyens C (2018) Additive manufacturing of powdery ni-based superalloys Mar-M-247 and CM 247 LC in hybrid laser metal deposition. *Metall Mater Trans A Phys Metall Mater Sci* 49:3812–3830. <https://doi.org/10.1007/s11661-018-4777-y>
2. Wang X, Carter LN, Pang B, Attallah MM, Loretto MH (2017) Microstructure and yield strength of SLM-fabricated CM247LC Ni-Superalloy. *Acta Mater* 128:87–95. <https://doi.org/10.1016/j.actamat.2017.02.007>
3. Boswell JH, Clark D, Li W, Attallah MM (2019) Cracking during thermal post-processing of laser powder bed fabricated CM247LC Ni-superalloy. *Mater Des* 174:107793. <https://doi.org/10.1016/j.matdes.2019.107793>
4. Kulkarni A (2018) Additive manufacturing of nickel based superalloys. *ArXiv* 1–12. <https://doi.org/10.31399/asm.hb.v24.a0006582>
5. Harris K, Erickson GL, Schwer RE (1984) MAR M 247 Derivations - CM 247 LC DS alloy. *C Single Cryst Alloy Prop Perform* 221–230
6. Basak A, Das S (2017) Microstructure of nickel-base superalloy MAR-M247 additively manufactured through scanning laser epitaxy (SLE). *J Alloys Compd* 705:806–816. <https://doi.org/10.1016/j.jallcom.2017.02.013>
7. Wang X, Carter LN, Adkins NJ, Essa K, Attallah MM (2020) Novel hybrid manufacturing process of CM247LC and multi-material blisks. *Micromachines* 11. <https://doi.org/10.3390/M111050492>
8. Chen Y, Zhang K, Huang J, Hosseini SRE, Li Z (2016) Characterization of heat affected zone liquation cracking in laser additive manufacturing of Inconel 718. *Mater Des* 90:586–594. <https://doi.org/10.1016/j.matdes.2015.10.155>
9. MacDonald JE, Khan RHU, Aristizabal M, Essa KEA, Lunt MJ, Attallah MM (2019) Influence of powder characteristics on the microstructure and mechanical properties of HIPped CM247LC Ni superalloy. *Mater Des* 174:107796. <https://doi.org/10.1016/j.matdes.2019.107796>
10. Henderson MB, Arrell D, Larsson R, Heobel M, Marchant G (2004) Nickel based superalloy welding practices for industrial gas turbine applications. *Sci Technol Weld Join* 9:13–21. <https://doi.org/10.1179/136217104225017099>
11. Jinoop AN, Paul CP, Bindra KS (2019) Laser-assisted directed energy deposition of nickel super alloys: a review. *The Proceedings of the Institution of Mechanical Engineers, Part L: Journal of Materials: Design and Applications* 233:2376–2400. <https://doi.org/10.1177/1464420719852658>
12. Graybill B, Li M, Malawey D, Ma C, Alvarado-Orozco JM, Martinez-Franco E (2019) Additive manufacturing of nickel-based superalloys 1–17

13. Pleass C, Jothi S (2018) Influence of powder characteristics and additive manufacturing process parameters on the microstructure and mechanical behaviour of Inconel 625 fabricated by Selective Laser Melting. *Addit Manuf* 24:419–431. <https://doi.org/10.1016/j.addma.2018.09.023>
14. Weng F, Gao S, Jiang J, Wang JJ, Guo P (2019) A novel strategy to fabricate thin 316L stainless steel rods by continuous directed energy deposition in Z direction. *Addit Manuf* 27:474–481. <https://doi.org/10.1016/j.addma.2019.03.024>
15. Forsey AN, Das YB, Simm TH, Clarke D, Boswell J, Gungor S, Moat RJ (2018) Mechanical property heterogeneity in additively manufactured nickel superalloy. *Mater Sci Eng A* 712:681–684. <https://doi.org/10.1016/j.msea.2017.12.025>
16. Jiménez A, Bidare P, Hassanin H, Tarlochan F, Dimov S, Essa K (2020) Powder-based laser hybrid additive manufacturing of metals: a review. *Int J Adv Manuf Technol*
17. Li Y, Feng Z, Hao L, Huang L, Xin C, Wang Y, Bilotti E, Essa K, Zhang H, Li Z, Yan F (2020) A review on functionally graded materials and structures via additive manufacturing: from multi-scale design to versatile functional properties. *Adv Mater Technol* 5. <https://doi.org/10.1002/admt.201900981>
18. Yuan K, Guo W, Li P, Wang J, Su Y, Lin X, Li Y (2018) Influence of process parameters and heat treatments on the microstructures and dynamic mechanical behaviors of Inconel 718 superalloy manufactured by laser metal deposition. *Mater Sci Eng A* 721:215–225. <https://doi.org/10.1016/j.msea.2018.02.014>
19. Hsu K-T, Wang H-S, Chen H-G, Chen P-C (2016) Effects of the hot isostatic pressing process on crack healing of the laser repair-welded CM247LC superalloy. *Metals (Basel)* 6:238. <https://doi.org/10.3390/met6100238>
20. Divya VD, Muñoz-Moreno R, Messé OMDM, Barnard JS, Baker S, Illston T, Stone HJ (2016) Microstructure of selective laser melted CM247LC nickel-based superalloy and its evolution through heat treatment. *Mater Charact* 114:62–74. <https://doi.org/10.1016/j.matchar.2016.02.004>
21. Bhaduri D, Penchev P, Essa K, Dimov S, Carter LN, Pruncu CI, Pullini D (2019) Evaluation of surface/interface quality, microstructure and mechanical properties of hybrid additive-subtractive aluminium parts. *CIRP Ann* 68:237–240. <https://doi.org/10.1016/j.cirp.2019.04.116>
22. Bhaduri D, Penchev P, Carter L, Essa K, Dimov S, Adkins N, Bajolet J, Tommasi A, Pullini D, Jurdeczka U (2018) Development and evaluation of a hybrid additive-subtractive process chain. In: *CIRP Winter Meet*
23. Mehmeti A, Penchev P, Lynch D, Vincent D, Maillol N, Maurath J, Bajolet J, Wimpenny DI, Essa K, Dimov S (2020) Mechanical behaviour and interface evaluation of hybrid MIM/PBF stainless steel components. *Rapid Prototyp J* 26(10):1809–1825. <https://doi.org/10.1108/RPJ-10-2019-0256>
24. Essa K, Modica F, Imbaby M, El-Sayed MA, ElShaer A, Jiang K, Hassanin H (2017) Manufacturing of metallic micro-components using hybrid soft lithography and micro-electrical discharge machining. *Int J Adv Manuf Technol* 91:445–452. <https://doi.org/10.1007/s00170-016-9655-4>
25. Hassanin H, Modica F, El-Sayed MA, Liu J, Essa K (2016) Manufacturing of Ti–6Al–4V micro-implantable parts using hybrid selective laser melting and micro-electrical discharge machining. *Adv Eng Mater* 18:1544–1549. <https://doi.org/10.1002/adem.201600172>
26. Careri F, Umbrello D, Essa K, Attallah MM, Imbrogno S (2019) The effect of the heat treatments on the tool wear of hybrid additive manufacturing of IN718. *Wear* 115800. <https://doi.org/10.1016/j.wear.2021.203617>
27. Imbrogno S, Alhuzaim A, Attallah MM (2021) Influence of the laser source pulsing frequency on the direct laser deposited Inconel 718 thin walls. *J Alloys Compd* 856. <https://doi.org/10.1016/j.jallcom.2020.158095>
28. M.-H. Multi-tasking, INTEGREX i-400S AM (n.d.). <https://www.mazakusa.com/machines/integrex-i-400s-am/>. Accessed 5 May 2022
29. Sow MC, De Terris T, Castelnao O, Hamouche Z, Coste F, Fabbro R, Peyre P (2020) Influence of beam diameter on laser powder bed fusion (L-PBF) process. *Addit Manuf* 36:101532. <https://doi.org/10.1016/j.addma.2020.101532>
30. Read N, Wang W, Essa K, Attallah MM (2015) Selective laser melting of AlSi10Mg alloy: process optimisation and mechanical properties development. *Mater Des* 65:417–424. <https://doi.org/10.1016/j.matdes.2014.09.044>
31. Hentschel O, Scheitler C, Fedorov A, Junker D, Gorunov A, Haimerl A, Merklein M, Schmidt M (2017) Experimental investigations of processing the high carbon cold-work tool steel 1.2358 by laser metal deposition for the additive manufacturing of cold forging tools. *J Laser Appl* 29:022307. <https://doi.org/10.2351/1.4983247>
32. Shamsaei N, Yadollahi A, Bian L, Thompson SM (2015) An overview of direct laser deposition for additive manufacturing; Part II: Mechanical behavior, process parameter optimization and control. *Addit Manuf* 8:12–35. <https://doi.org/10.1016/j.addma.2015.07.002>
33. Carter LN, Attallah MM, Reed RC (2012) Laser powder bed fabrication of nickel-base superalloys: influence of parameters; characterisation, quantification and mitigation of cracking. *Superalloys* 2012:577–586. <https://doi.org/10.1002/9781118516430.ch64>

Publisher's Note Springer Nature remains neutral with regard to jurisdictional claims in published maps and institutional affiliations.